

Hadronic structure in $\tau^- \rightarrow \pi^- \pi^- \pi^+ \nu_\tau$ decays

Edward I. Shibata^a *

^aDepartment of Physics, Purdue University,
West Lafayette, Indiana 47907-2036, United States of America

A model-dependent analysis of the hadronic substructure in $\tau^- \rightarrow \pi^- \pi^- \pi^+ \nu_\tau$ decay is reported. The decay is dominated by the process $\tau^- \rightarrow a_1^-(1260) \nu_\tau$, in which $a_1^-(1260) \rightarrow \rho^0 \pi^-$ in an S -wave decay. Amplitudes involving $a_1(1260)$ decays into isoscalars, especially $a_1(1260)^- \rightarrow f_0(600) \pi^-$, are large. $\tau^- \rightarrow \pi^- \pi^- \pi^+ \nu_\tau$ decays via the pseudoscalar $\pi^-(1300)$ are small. These results support the resonant substructure reported in the previously reported analysis of $\tau^- \rightarrow \pi^0 \pi^0 \pi^- \nu_\tau$ decay mode from the same CLEO II data sample.

1. INTRODUCTION

The $\tau^- \rightarrow (3\pi)^- \nu_\tau$ decay has been the subject of much interest over the years. Because of the transformation properties of the weak current under parity and G -parity, τ -lepton decay to an odd number of pions is expected to occur exclusively through the axial vector current, ignoring isospin-violating effects. Since J^P , and I^G are good quantum numbers of the hadronic current from weak decays, the weak axial current produces systems of pions with $J^P = 0^-$ or 1^+ , odd G -parity and odd numbers of pions.

The $(3\pi)^-$ system in $\tau^- \rightarrow (3\pi)^- \nu_\tau$ is expected to be produced dominantly through the poorly understood $J^P = 1^+$ $a_1^-(1260)$ where $a_1^-(1260) \rightarrow \rho^0 \pi^-$ in an S -wave decay. Although it is possible that the $(3\pi)^-$ system can be produced through the $J^P = 0^-$ $\pi^-(1300)$, this is expected to be suppressed by the PCAC (partially conserved axial current) hypothesis. It has been known for some time that simple models do not provide a satisfactory description. For example, ARGUS [1] found that the model of Kühn and Santamaria [2] and that of Isgur, Morningstar, and Reader [3] did not describe their $\tau^- \rightarrow (3\pi)^- \nu_\tau$ data satisfactorily.

Here we report the preliminary results of a model-dependent fit of the substructure in $\tau^- \rightarrow \pi^- \pi^- \pi^+ \nu_\tau$ decays. The work is based on the analysis of $\sim 145,000$ $\tau^- \rightarrow \pi^- \pi^- \pi^+ \nu_\tau$ events

[4]. In addition to fitting the substructure with various $a_1^-(1260)$ decay modes, fits for the production of the $(3\pi)^-$ system via the $J^P = 0^-$ $\pi^-(1300)$ are included. These results are compared to the substructure in $\tau^- \rightarrow \pi^0 \pi^0 \pi^- \nu_\tau$ previously reported [5].

Throughout this paper the charge conjugate versions of decays are implied for brevity and clarity.

2. EVENT SELECTION

This analysis is based on 4.67 fb^{-1} of e^+e^- colliding beam data collected at center-of-mass energy energies $E_{cm} \sim 10.6 \text{ GeV}$ with the CLEO II detector at the Cornell Electron Storage Ring (CESR). This corresponds to 4.3×10^6 $e^+e^- \rightarrow \tau^+\tau^-$ events. $\tau^- \rightarrow \pi^- \pi^- \pi^+ \nu_\tau$ events are selected from a topology in which the τ^+ decays into a single charged particle plus a $\bar{\nu}_\tau$ and the τ^- decays into three charged particles plus a ν_τ (1 versus 3 charged-particle topology). Selected events are required to have four well-constructed charged tracks coming from the interaction region, and the net charge of the tracks is required to be zero. No more than one track is allowed to be identified as an e^- or e^+ . The most isolated track is identified, and the remaining three tracks are required to be $\geq 90^\circ$ away from it. Events with photons (isolated electromagnetic showers not associated with a track) are rejected. Events that satisfy the hypothesis $0.485 < M_{\pi^+\pi^-} <$

*representing the CLEO Collaboration.

0.510 GeV are rejected in order to eliminate events containing $K_s^0 \rightarrow \pi^+\pi^-$ decays. Finally, the 2-dimensional cut shown in Figure 1 is used to reject events with missing tracks and/or energy along the beam pipe. Application of these cuts yields 145,000 $\tau^- \rightarrow \pi^-\pi^-\pi^+\nu_\tau$ events.

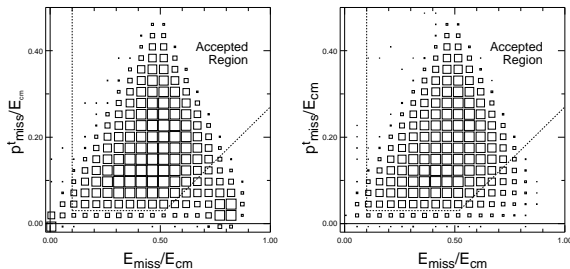


Figure 1. E_{miss}/E_{cm} vs. p_{miss}^t/E_{cm} for experimental data (left) and Monte Carlo τ -events (right), where E_{miss} is the missing energy and p_{miss}^t is the missing transverse momentum in an event. This 2-dimensional cut is used to reject events with missing tracks and/or energy along the beam axis.

The $\pi^-\pi^-\pi^+$ effective mass spectrum resulting from these cuts is shown in Figure 2. The background, indicated by the shaded histogram, which amounts to about 11% of the events in the spectrum. Monte Carlo studies show that this background is from other τ -decays: $\sim \frac{1}{2}$ comes from τ -events with missing π^0 (’s) and $\sim \frac{1}{2}$ is from τ -events with ≥ 1 charged K . Monte Carlo studies indicate that backgrounds from multihadronic $q\bar{q}$ events, $\gamma\gamma$ events, and QED events are negligible.

3. FIT

Although it is desirable to characterize the structure of the $\pi^-\pi^-\pi^+$ system without model-dependent assumptions, this is very difficult in practice. In a model-independent approach one would assume a general form of the hadronic current that allows the separation and analysis of the complex magnitudes of the axial vector and

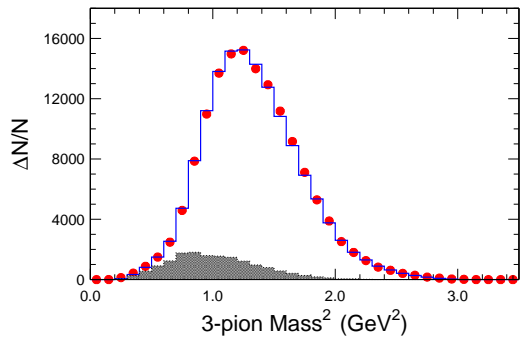


Figure 2. $\pi^+\pi^+\pi^-$ effective mass spectrum. The circles are the experimental data and the histogram is the spectrum resulting from fitting the data sample as described in the text. The shaded histogram is the background from other τ decays.

pseudoscalar components in bins of Q^2 , s_1 , and s_2 , where Q^2 is the invariant mass-squared of the $\pi^-\pi^-\pi^+$ system, s_1 is the invariant mass-squared of the $\pi^+\pi^-$ combination that yields the larger value of mass-squared, and s_2 is the invariant mass-squared of the other $\pi^+\pi^-$ combination. There would be no assumptions regarding resonances in the decay. However, in certain chiral limits, scalar effects can be induced in the current from the $a_1^-(1260)$ and non-resonant contributions in the current and thus fake pseudoscalar effects [8]. Secondly, simply binning in three dimensions is problematical: relatively small bins are required to study the τ decay structure and this leads to some bins with low statistics that may be crucial in resolving complicated resonance structure. By using a model-dependent fit, one can make reasonable assumptions about the resonant structure and study the likely existence of each resonance modeled while using the entire dataset in the fitting and without the need for binning.

Using an unbinned maximum likelihood fit, the substructure in $\tau^- \rightarrow \pi^-\pi^-\pi^+\nu_\tau$ decays has been fit with the set of resonances given in Table 1. For comparison purposes, the current Particle Data

Table 1

Masses and widths of the resonances used in the fits to $\tau^- \rightarrow \pi^- \pi^- \pi^+ \nu_\tau$ and $\tau^- \rightarrow \pi^0 \pi^0 \pi^- \nu_\tau$ decays. For comparison the current Particle Data Group [6] masses and widths are listed.

Particle	$I^G(J^{PC})$	M (GeV)	Γ (GeV)	M_{PDG} (GeV)	Γ_{PDG} (GeV)
$a_1(1260)$	$1^-(1^{++})$	1.230	0.400	1.23 ± 0.04	0.25–0.60
$\pi(1300) = \pi'$	$1^-(0^{-+})$	1.300	0.300	1.3 ± 0.1	0.2–0.6
$\rho(770)$	$1^+(1^{--})$	0.774	0.149	0.7711 ± 0.0009	0.1492 ± 0.0007
$\rho(1450)$	$1^+(1^{--})$	1.370	0.386	1.465 ± 0.025	0.31 ± 0.06
$f_2(1270)$	$0^+(2^{++})$	1.275	0.185	1.2754 ± 0.0012	$0.1851^{+0.0034}_{-0.0026}$
$f_0(600) = \sigma$	$0^+(0^{++})$	0.860	0.880	0.4–1.2	0.6–1.0
$f_0(1370)$	$0^+(0^{++})$	1.186	0.350	1.2–1.5	0.2–0.5

Group [6] masses and widths are listed. For the $f_0(600)$ and $f_0(1370)$ resonance parameters given by the Törnqvist unitarized quark model [7] have been used. The same resonances and parameters have been used in the analysis of $\tau^- \rightarrow \pi^0 \pi^0 \pi^- \nu_\tau$ events [5] selected from the same CLEO II set of $e^+e^- \rightarrow \tau^+\tau^-$ events.

ture previously reported for the CLEO II $\tau^- \rightarrow \pi^0 \pi^0 \pi^- \nu_\tau$ [5] data, which are based on $\sim 15,000$ lepton-tagged events. The fit results on these events are given in Table 3 for the reader's convenience. Both analyses find that axial vector amplitudes with isoscalars, especially $a_1^-(1260) \rightarrow f_0(600)\pi^-$, are large.

4. RESULTS

The results of the fit are given in Table 3, where the β_i are complex coupling constants. The $\pi^- \pi^- \pi^+$ invariant mass spectrum resulting from the fit is shown as the histogram in Figure 2.

As expected, the $a_1^-(1260) \rightarrow \rho^0 \pi^-$ S -wave decay dominates. There is a significant amount of p -wave $a_1(1260)$ decay into isoscalars [$f_0(600)$, $f_0(1370)$] plus a pion. τ -decay via the pseudoscalar $\pi^-(1300)$ is small, although its inclusion improves the fit. Dalitz plots for sequential $\pi^- \pi^- \pi^+$ invariant mass regions are shown in Figure 3 for data and the fit.

The isoscalar sub-resonances in the decay of the $a_1^-(1260)$ [$f_0(600)$, $f_2(1270)$, and $f_0(1370)$] play a large role in the fits. To demonstrate the need for these isoscalars, the data were fitted without them. Projections of the Dalitz plot without the presence of these isoscalars are shown in Figures 6 and 7. For the projection onto the s_1 axis (Figure 6), the lack of all three isoscalars results in a poor fit for $Q^2 \geq 2.25$ GeV². For the projection onto the s_2 axis (Figure 7), the presence of $f_0(600)$ is needed for all regions of Q^2 , especially those of lower Q^2 values.

These results support the resonance substruc-

Table 2

Preliminary results based on $\sim 145,000$ $\tau^- \rightarrow \pi^- \pi^- \pi^+ \nu_\tau$ events. The uncertainties are statistical only. The branching fractions do not sum to 100% due to interferences among the amplitudes. The phases are relative to the dominant $a_1(1260) \rightarrow \rho\pi$ s -wave decay.

		Branching fraction (%)	$\mathcal{R}e(\beta)$	$\mathcal{I}m(\beta)$
$a_1 \rightarrow \rho\pi$	S -wave	69.77	1.00	0.0
$a_1 \rightarrow \rho(1450)\pi$	S -wave	1.58 ± 0.25	0.05 ± 0.02	-0.25 ± 0.02
$a_1 \rightarrow \rho\pi$	D -wave	1.68 ± 0.16	0.61 ± 0.03	0.35 ± 0.05
$a_1 \rightarrow \rho(1450)\pi$	D -wave	2.77 ± 0.29	-1.60 ± 0.11	-1.21 ± 0.10
$a_1 \rightarrow f_2(1270)\pi$	P -wave	0.68 ± 0.08	-0.12 ± 0.07	0.96 ± 0.06
$a_1 \rightarrow f_0(600)\pi$	P -wave	48.40 ± 1.61	1.99 ± 0.06	2.70 ± 0.06
$a_1 \rightarrow f_0(1370)\pi$	P -wave	11.51 ± 0.82	-0.04 ± 0.04	-1.15 ± 0.04
$\pi(1300) \rightarrow \rho\pi$	P -wave	0.01 ± 0.02	0.001 ± 0.002	-0.002 ± 0.001
$\pi(1300) \rightarrow \rho(1450)\pi$	P -wave	0.02 ± 0.03	-0.005 ± 0.010	-0.013 ± 0.009
$\pi(1300) \rightarrow f_0(600)\pi$	S -wave	0.13 ± 0.07	-0.005 ± 0.003	-0.008 ± 0.002

Table 3

Results for the substructure fit to $\sim 15,000$ lepton-tagged $\tau^- \rightarrow \pi^0 \pi^0 \pi^- \nu_\tau$ events from the same CLEO II $e^+e^- \rightarrow \tau^+\tau^-$ dataset. The branching fractions do not sum to 100% due to interferences among the amplitudes.

		Significance	Branching fraction (%)	$ \beta $	phase φ/π
$\rho\pi$	S -wave	–	68.11	1.00	0.0
$\rho(1450)\pi$	S -wave	1.4σ	0.30 ± 0.64	0.12 ± 0.09	0.99 ± 0.25
$\rho\pi$	D -wave	5.0σ	0.36 ± 0.17	0.37 ± 0.09	-0.15 ± 0.10
$\rho(1450)\pi$	D -wave	3.1σ	0.43 ± 0.28	0.87 ± 0.29	0.53 ± 0.16
$f_2(1270)\pi$	P -wave	4.2σ	0.14 ± 0.06	0.71 ± 0.16	0.56 ± 0.10
$f_0(600)\pi$	P -wave	8.2σ	16.18 ± 3.85	2.10 ± 0.27	0.23 ± 0.03
$f_0(1370)\pi$	P -wave	5.4σ	4.29 ± 2.29	0.77 ± 0.14	-0.54 ± 0.06

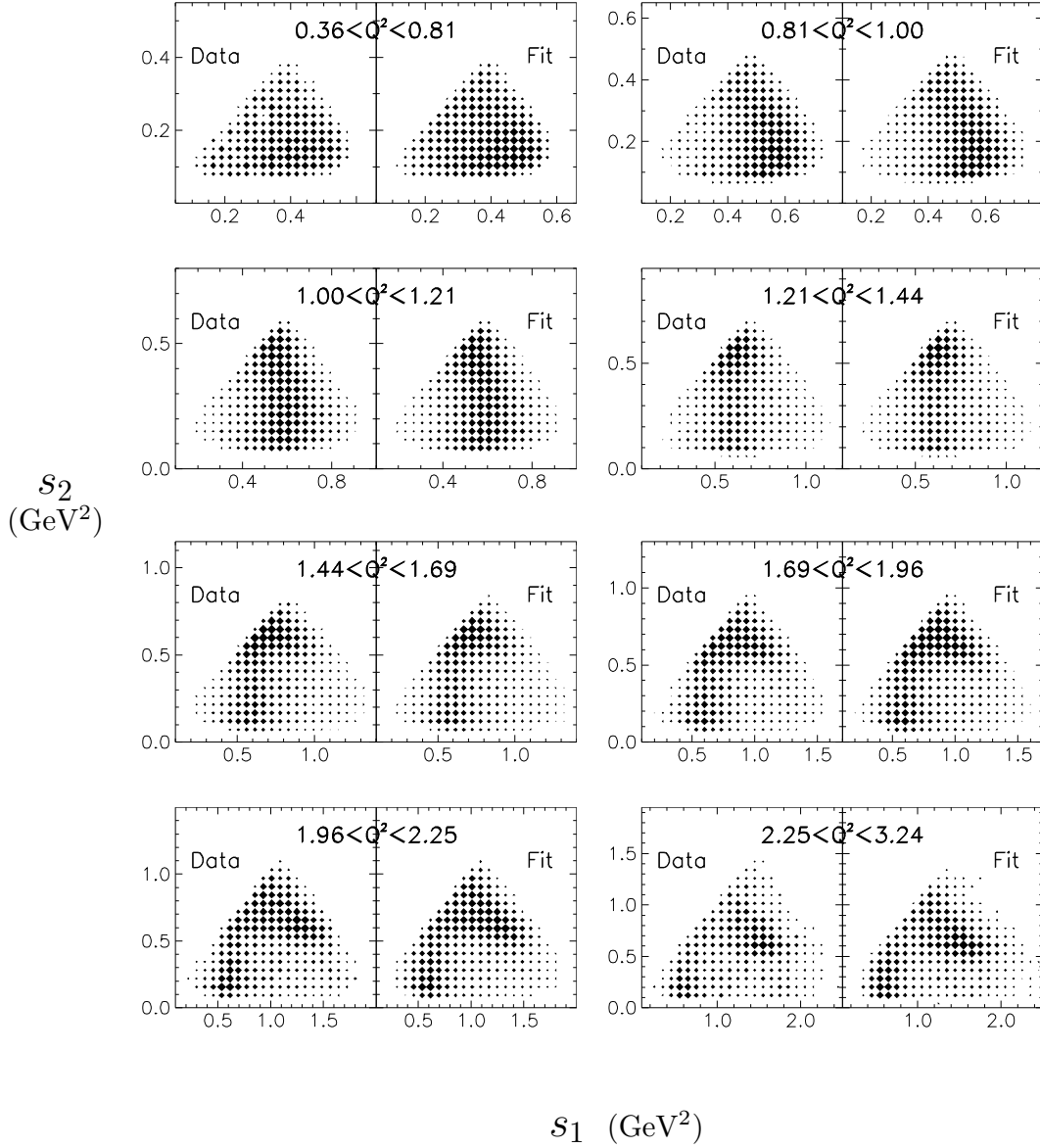


Figure 3. Dalitz plots for sequential bins in $Q^2 = M_{\pi^-\pi^-\pi^+}^2$. Q^2 is in units of $(\text{GeV})^2$. s_1 and s_2 are the two possible $\pi^+\pi^-$ invariant masses squared; s_1 is the larger of the two possible $\pi^+\pi^-$ invariant mass-squared values.

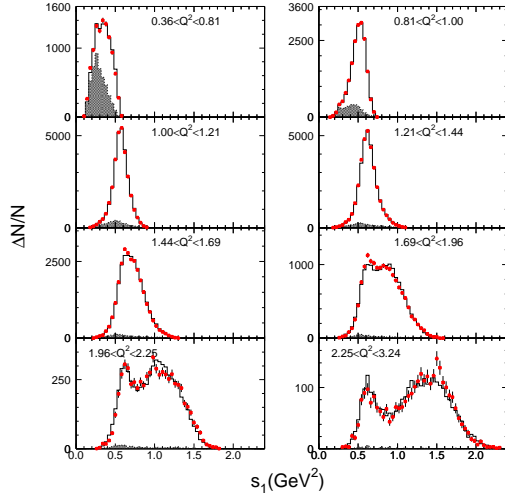


Figure 4. Projection of the Dalitz plot onto the $s_1 = M_{\pi^+\pi^-}^2$ axis for various bins in $M_{3\pi}^2$. The points are the experimental data and the histogram is the result of the fit. The shaded regions represent the background.

5. SUMMARY

This work is a new measurement of substructure in $\tau^- \rightarrow \pi^- \pi^- \pi^+ \nu_\tau$. A model-dependent unbinned maximum likelihood fit on 145,000 events was performed using an axial vector component [$a_1(1260)$ primary resonance and several subresonances, including isoscalars] and a pseudoscalar component [$\pi(1300)$ plus several subresonances]. As expected, this decay is dominated by $\tau^- \rightarrow a_1^-(1260)\nu_\tau$ with subsequent $a_1 \rightarrow \rho^0\pi^-$ S -wave decay. However, it is also apparent that other $a_1^-(1260)$ decay modes are present. In particular, $a_1^-(1260)$ decay into isoscalars [$f_0(600)$, $f_2(1270)$, and $f_0(1370)$] is significant. The $a_1^-(1260) \rightarrow f_0(600)\pi^-$ is especially prominent. These results are consistent with the earlier CLEO II results for $\tau^- \rightarrow \pi^0\pi^0\pi^-\nu_\tau$ [5]. Both analyses find that axial-vector amplitudes with isoscalars, especially $a_1^-(1260) \rightarrow f_0(600)\pi^-$, are large. Regarding non-axial-vector contributions, inclusion of the

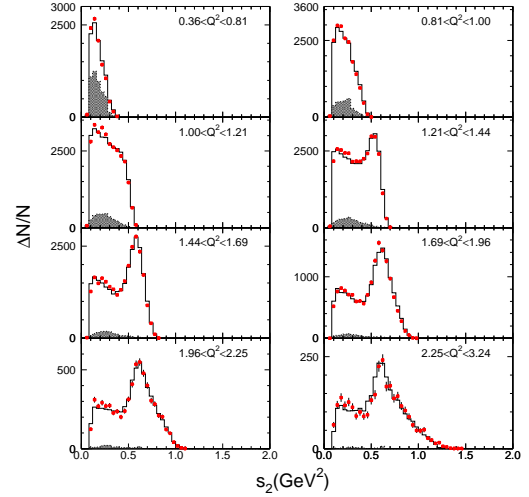


Figure 5. Projection of the Dalitz plot onto the $s_2 = M_{\pi^+\pi^-}^2$ axis for various bins in $M_{3\pi}^2$. The points are the experimental data and the histogram is the result of the fit. The shaded regions represent the background.

$J^P = 0^- \pi^-(1300)$ improves the fit to the data in the expected regions, but the need for it is not compelling. It is hoped that the future CLEO-c dataset will clarify some of these issues.

6. ACKNOWLEDGEMENTS

This work represents the work of many CLEO collaborators, especially Jason W. Hinson, Jon Urheim, and Alan J. Weinstein. The CESR staff provided us with excellent luminosity and running conditions. This work is supported by the National Science Foundation, the U. S. Department of Energy, and the Natural Sciences and Engineering Research Council of Canada.

REFERENCES

1. H. Albrecht et al., Phys. Lett. B349 (1995) 576.
2. J. H. Kühn and A. Santamaria, Z. Phys. C 48 (1990) 445.

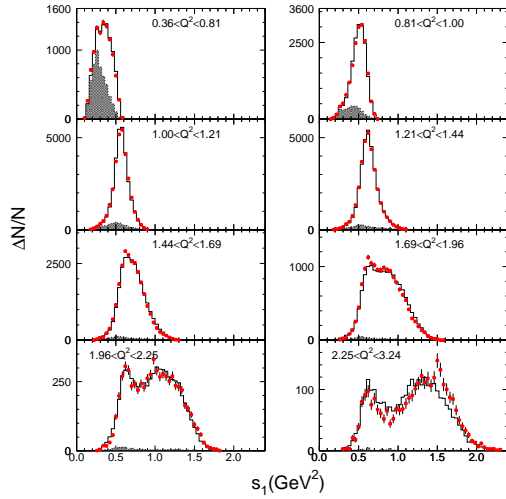


Figure 6. Projection of the Dalitz plot onto the $s_1 = M_{\pi^+\pi^-}^2$ axis for various bins in $M_{3\pi}^2$ for a fit without isoscalars. The points are the experimental data and the histogram is the result of the fit. The shaded regions represent the background.

3. N. Isgur, C. Morningside, and C. Reader, Phys. Rev. D39 (1989) 1357.
4. J. W. Hinson, Ph.D. thesis, Purdue University (2001), PU-99-713.
5. D. M. Asner et al., Phys. Rev. D61 (1999), 012002, hep-ex/9902022.
6. K. Hagiwara et al., Phys. Rev. D66 (2002), 010001.
7. N. A. Törnqvist, Z. Phys. C 68 (1995), 647–660.
8. R. Decker, M. Finkemeier, and E. Mirkes, Phys. Rev. D50 (1994) 6863, hep-ph/9310270.

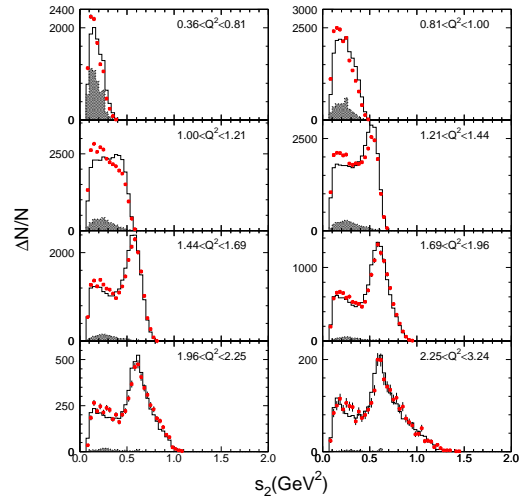


Figure 7. Projection of the Dalitz plot onto the $s_2 = M_{\pi^+\pi^-}^2$ axis for various bins in $M_{3\pi}^2$ for a fit without isoscalars. The points are the experimental data and the histogram is the result of the fit. The shaded regions represent the background.